CFD Investigation for Effect of the Aerodynamic Truck - Cabin Profiles and Devices on the Truck Performance

E. S. Abdelghany [1]

***Abstract*-- Today's request for reducing the fuel consumption of Heavy vehicles is one of the most interesting issues within the automotive industry. Together with the increased fuel price, the development of more fuel efficient vehicles has intensified. Recent research about fuel-saving technologies for trucks displayed that aerodynamic improvement is one of the most essential technologies when it comes to reducing fuel. The Main objective of this study is to determine the aerodynamic impact (drag force) for various profiles in the truck - cabin shape and Aerodynamic devices added in truck cabin such as, [Cap of truck (with different angle), Gap device (with different length)]. To measure the aerodynamic drag produced by the truck, numerical model studies are undertaken using a 1/50 scale model of standard heavy truck. In this research, a numerical validation procedure by ANSYS FLUENT ®, computational fluid dynamics software with various turbulence models is described for estimation aerodynamic characteristics. It is observed that at the present work a good agreement between the numerical study and the experimental work with the Realizable k-ε model with maximum error is about 8%.**

Then, computational fluid dynamic (CFD) investigation is utilized for each case to compare with respect to coefficient of drag, Turbulence Kinetic Energy contours, pressure contours, velocity contours, 3D streamlines and velocity vectors between a standard 3D truck model with and without aerodynamic profiles and devices. The results show that the front and mid fillet radius profile has a significant drag coefficient reduction is noticed by about 17.75% with optimum dimensions. The top fillet radius profile has an opposite effect on the drag coefficient due to the Coandă Effect without cap of truck. When top fillet radius is utilized with a cap of the truck, the drag coefficient improvement with an optimism cap truck angle by about 9.92%. By adding Gap device with different lengths, the drag coefficient decreasing by about 8.36%. Finally, by using all aerodynamic profiles and devices on the truck - cabin studied at the same time the improvement in drag coefficient is about 36.03% from a standard 3D truck model.

***Index Term*--** Aerodynamics**, CFD, Drag reduction, Truck – Cabin profiles, fuel consumption.**

1. INTRODUCTION

The heavy commercial vehicles have high fuel consumption, in comparison to other ground vehicles, due to high aerodynamic drag, [1], [2] and [3]. The fuel reduction technologies for trucks show that aerodynamic development is one of the most significant technologies when it comes to fuel decreasing. The main cause of truck aerodynamic drag is due to form drag (pressure drag). Pressure drag on trucks due to flow separation establishes more than 80% of the total aerodynamic drag, while frictional drag establishes for the remaining 20%. Thus, decreasing aerodynamic drag is significant for the fuel saving, [4] and [5].

The fuel consumption is an important issue in the road transport industry; the Centre for Transportation Analysis calculated that medium and heavy trucks consumed 6012 trillion BTU (British thermal unit) in the US during 2014, which is the 23% of Domestic Transportation Energy (DTE), being the second largest consumers after the light vehicles category, as shown in fig. 1. If the average of drag losses of heavy vehicles were 20%, the drag losses would represent 4.6% of the DTE, which would be equivalent to 1204 trillion BTU. This means that any improvement in aerodynamic will represent an important fuel saving, [6].

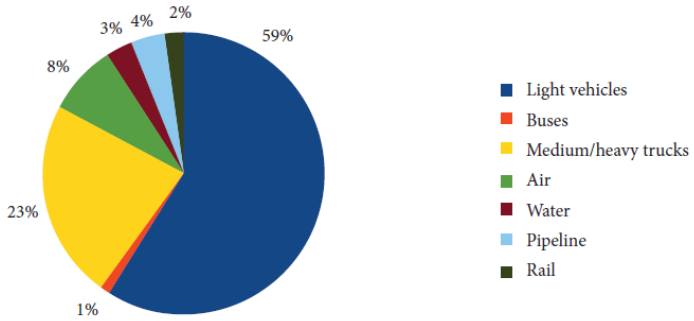

Fig. 1. Percentages of domestic consumption of transportation energy in the US during 2014, [6].

From [7], It is investigated numerous aerodynamic retrofitting techniques to decrease heavy vehicle fuel consumption. The numerical models are used to simulate realistic on-road operations to show the effect of retrofits on various vehicle weights and driving cycles. The results are shown that the fuel economy improvement could be accomplished from less than 1% to almost 9% of annual mileage. From [8], a numerical simulation is investigated unsteady aerodynamic flows affecting the fuel consumption of Class 8 trucks and is validated their results with comparison to experimental data. from [9], The

[1] Mechanical Engineering Departement. Faculty of Engineering, Albaha University KSA, on Leave from Institute of Aviation Engineering and Technology, Giza , Egypt, Eslam_said312002@yahoo.com.

computational fluid dynamic (CFD) analysis is used to investigate the effects of adding append devices like deflector, cab vane corner, Cab/trailer gap, Front fairing, Back vane and Base flap on heavy commercial vehicle drag reduction. It is found about 41% drag reduction by installing all supplementary parts at their optimized positions. From [10], the numerical models with Shear tress transportation (SST) turbulence model is used to investigate both unmodified and modified profile of the truck-trailer. The results showed that the profile modification cases decrease in aerodynamic drag up to 21 %, which decreases the fuel consumption by 4 liters for 100 km for the diesel-powered truck. From [11], it is carried out a CFD study in order to design and optimize the cabin geometry and its various parts for drag decrease including the side deflectors, the mirrors, and the sun visor. From [12], a 1/10 the scale semi-trailer truck model is used in a wind tunnel at various speeds and yaw angles using different combinations of fairings to find drag reduction. It is found that any improvement in the front area of the truck has the most significant effect on drag. It is obtained a 26% drag reduction for the best combination. It is calculated that the cab roof fairing alone can reduce about 17% of drag, and if joined with the fairing for the tractor-trailer gap, the drag reduction can be up to 25.5%.

2. VALIDATION PROCEDERS

The main object of this research is to measure the aerodynamic drag force of the truck by experimental and numerical work. However, the experimental techniques are quite laborious and surely cost more than CFD techniques cost for the same. Computational fluid dynamics (CFD) has become tool for developing, supporting, optimizing, innovating, verifying and, especially, for validating procedures. Verifying and validating forerun steps for the code calibration procedure is investigated by [13]. In this research, it is taken a 1/50 scale detailed model of a standard heavy truck and it is measured the drag with velocity experimentally and numerically. It is clarified the aerodynamic impact of various profiles in the cabin truck shape and Aerodynamic devices added in truck cabin such as, [Cap of truck (with different angle), Gap filling (with different length)].

2.1. Experimental Set up

The institute of aviation engineering and technology has an open-circuit suction wind tunnel in the aerodynamics laboratory. The tunnel ducting is composed of four major duct components. The components are the settling chamber, contraction cone, the test section, the diffuser and then fan housing. The wind tunnel test section is 24 inch length and 12 × 12- Inch cross-section. The maximum velocity that can create around 30 m/s with 9 blade fan, as shown in Fig. 2. The wind tunnel has three-component sting balance. The sting balance is used to measure all two forces (drag, lift) and one moment at a time. The reading of the sting balance is indicated in the inductor panel, behind the panel signal conditioning cards, which convert the volt signals from the sting balance and pressure transducers to forces, moment, pressure, and velocity, as shown in fig. 2.

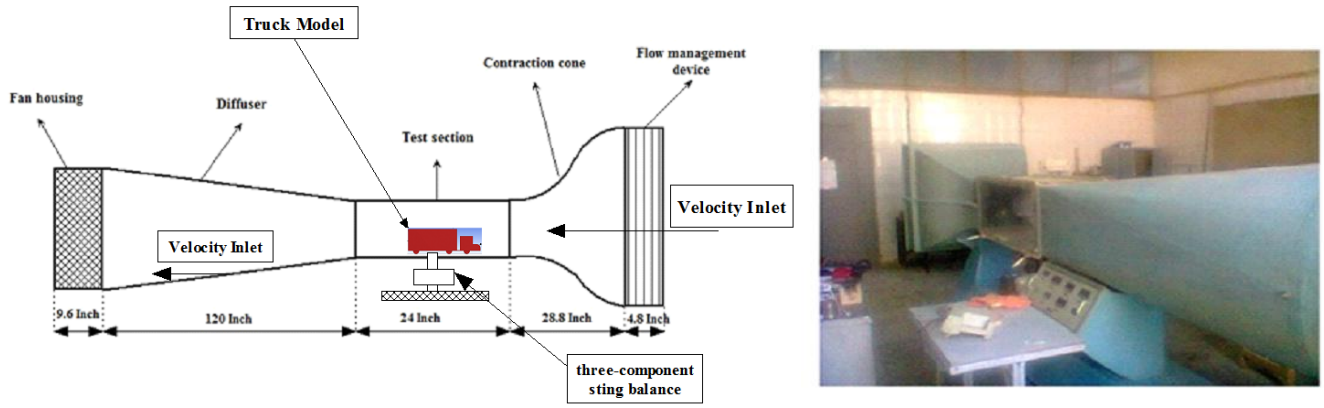

Fig. 2. Wind tunnel component photograph and dimensions.

In this research, only aerodynamic drag force (D) data and its dimensionless parameter drag coefficient (CD) are presented. The CD is calculated by using the following formula:

$$C_D = \frac{D}{0.5 \times \rho \times v^2 \times A} \quad (1)$$

Where: D is the drag force, A is project area of the truck, ρ and v are the density and air velocity

A one-fifty scale detailed model of a standard heavy truck is used as a baseline truck, as shown in fig. 3(b). From figure 3

(a), the model is placed in the test section of wind tunnel and it is measured drag forces with variable velocities (from 12 to 25 m/s). Several data collections are collected at each speed experienced and the results are averaged for minimizing the further possible errors in the raw experimental data.

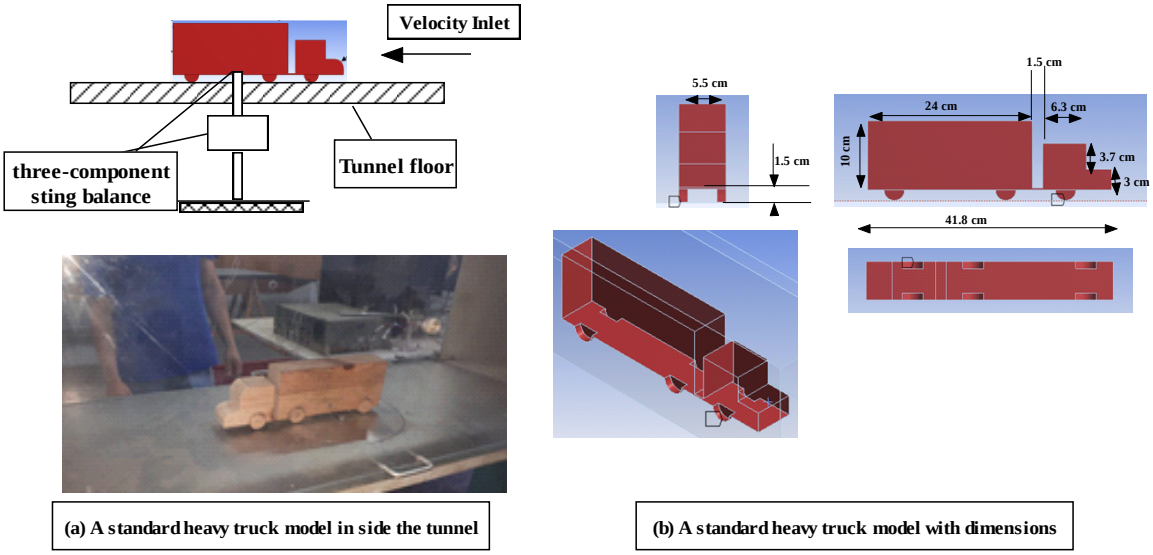

Fig. 3. A standard heavy truck model inside the tunnel.

2.2. Numerical Analysis

According to a standard heavy truck in experimental method, it is designated the same model dimensions, as shown in Fig. 3(b). The flow field, temperature, pressure and velocity inlet in the numerical model of 3D truck, are solved using ANSYS FLUENT@19.

2.2.1. Boundary Conditions and Meshing

At first, a standard heavy truck is modeled as two boxes by using Design modular and boundary conditions are defined. The Reynolds number (Re) for the velocity inlet boundary (number 1) is 5.75231×10^5, as shown in Fig 4. The same properties in the experimental work are used in the present simulation to validate the code. The free stream temperature is 300 K, which is the same as the environmental temperature. The density of the air at the given temperature is ρ=1.225kg/m3, the pressure is 101325 Pa and the viscosity is μ=1.7894×10-5 kg/m s. A segregated, implicit solver is utilized (ANSYS FLUENT® processor) Calculations are done for velocity ranging from 10 m/s to 25 m/s (Re from 350000 to 650000). The pressure outlet (number 2) is 101325 Pa as the environmental pressure. The Standard heavy truck profile (number 3) as shown in Fig 4, is considered adiabatic and no slip wall. The two vertical and horizontal planes around 3D truck are considered adiabatic and no slip wall, as shown in Fig 4.

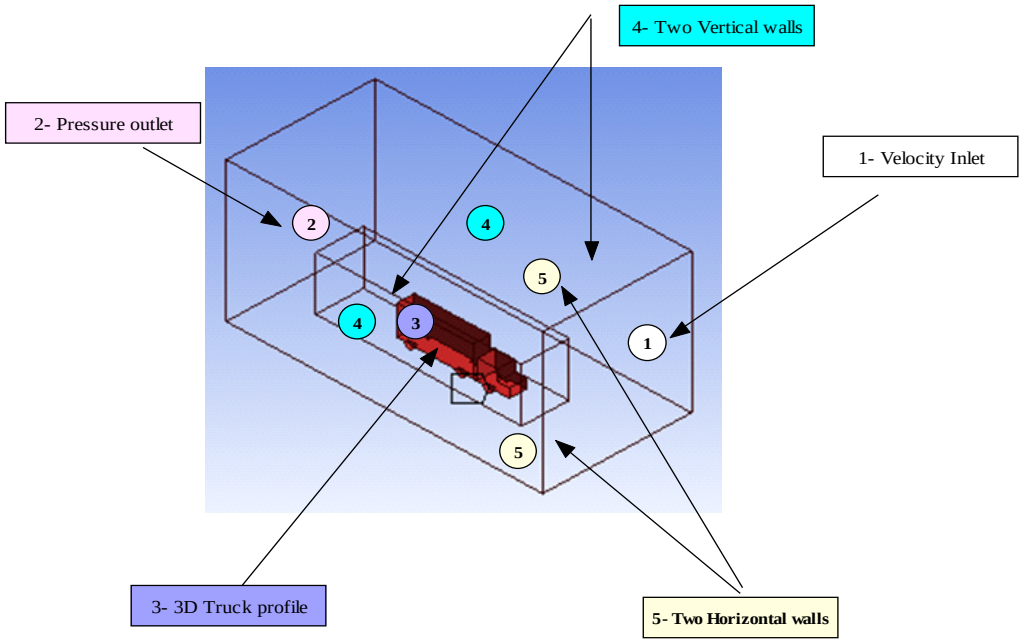

Fig. 4. Boundary Conditions of a Standard Truck model.

In order to obtain precise the drag force on a standard heavy truck, grids near the 3D truck volume must be dense sufficient and computed fields must be large sufficient to satisfy higher accuracy and reducing time. Using 3D unstructured tetrahedral mesh, increasing mesh cells, it is needed super computer and more time to solve the problem. Many researchers developed various methods and tools to overcome the problems described above. From [14, 15, 16 and 17], it is presented a number of grid generation methods to construct high quality single- and multi-block structure grid for complex shape. In present work using multi-block unstructured grid to increase grids near 3D truck volume by creating block around truck and making body inflation, as shown in fig 5. It is created face inflation and face sizing in truck volume faces which reduce the computational time and obtain accurate drag, as shown in fig 5.

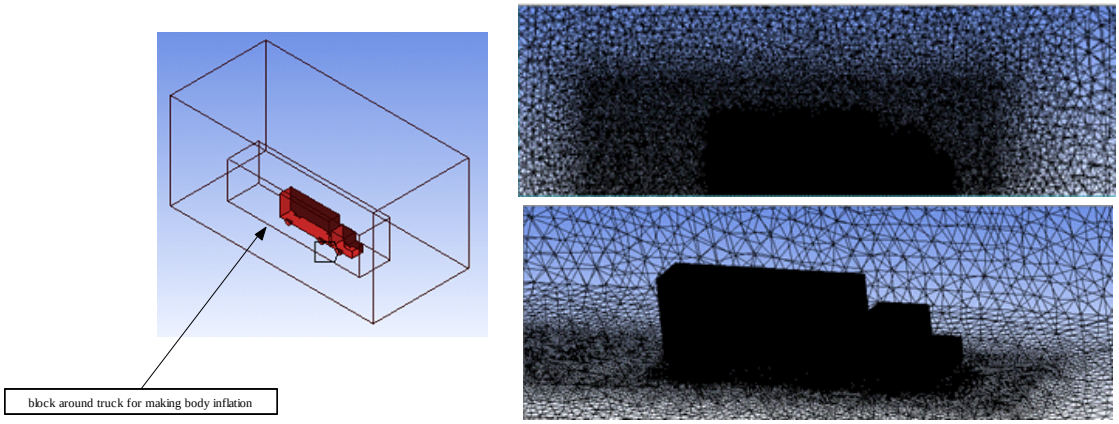

Fig. 5. A standard 3D truck of the meshed control volume (a) Multi Block Method for meshing the truck to generate body sizing (b) Mesh face sizing on truck surface.

The mesh is generated using ANSYS FLUENT MESH® 19 as a pre-processor and mesh generator. The body sizing is applied with a minimum element size of 1×10-4 m at the truck walls and it is processed a growth rate of 1.02 and a maximum element size of 0.1 m. The grid is of the unstructured tetrahedral-hybrid grid type. The meshed

control volume of block around 3D tuck volume is shown in Fig 5. The total number of cells in the full grid is about 3000000 cells.

2.2.2. Grid dependency check and Verification of Numerical Model

The first step in performing a CFD simulation should be to investigate the effect of the mesh size on the solution results. The appropriate number of nodes is determined by increasing the number of cells until the mesh is sufficiently fine, so that further refinement does not change the results. To examine the independence of the results to cell number, six kinds of mesh are generated. Figure 6 shows the effect of the number of grid cells in coefficient of drag at velocity inlet 20 m/s. It is taken 2500000 cells to reducing time of solution.

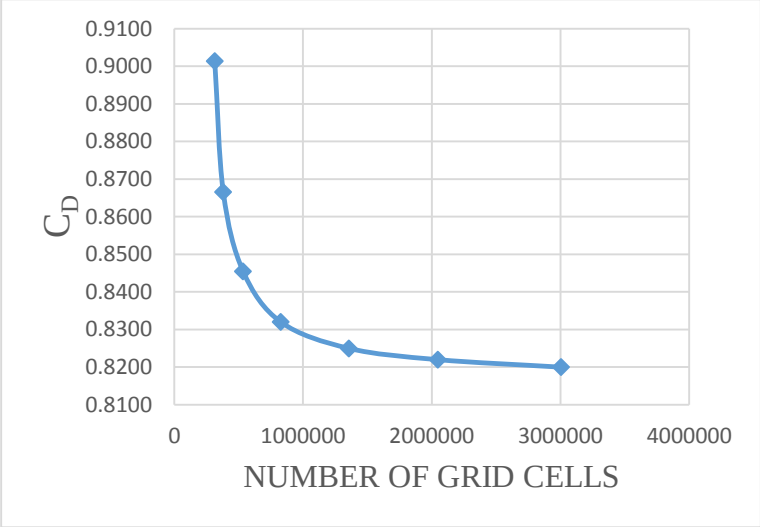

Fig. 6. Curve of drag coefficient at velocity inlet 20 m/s against number of grid cells.

A similar Numerical Model a standard heavy truck of the same previously-mentioned grid size and type is developed, for verifying numerical model with the experiment model study with the same boundary conditions, as shown in Fig 7. Compare the results of the numerical model by Realizable k – ε model with enhanced wall treatment, the standard model k–ω model and Spalart-Allmaras model to those of the experimental measurements. The results show a good agreement of a drag coefficient with the corresponding values in the experimental model measurements. Figure 7 shows the drag coefficient (CD) with velocity from 12 to 25 m/s (Reynolds number from 350000 to 650000) of numerical and experimental studies, plotted on the same axes and scale for comparison. It is found that the Realizable k – ε model with enhanced wall treatment model with a maximum error about 8% more accurately than k–ω and Spalart-Allmaras turbulence models.

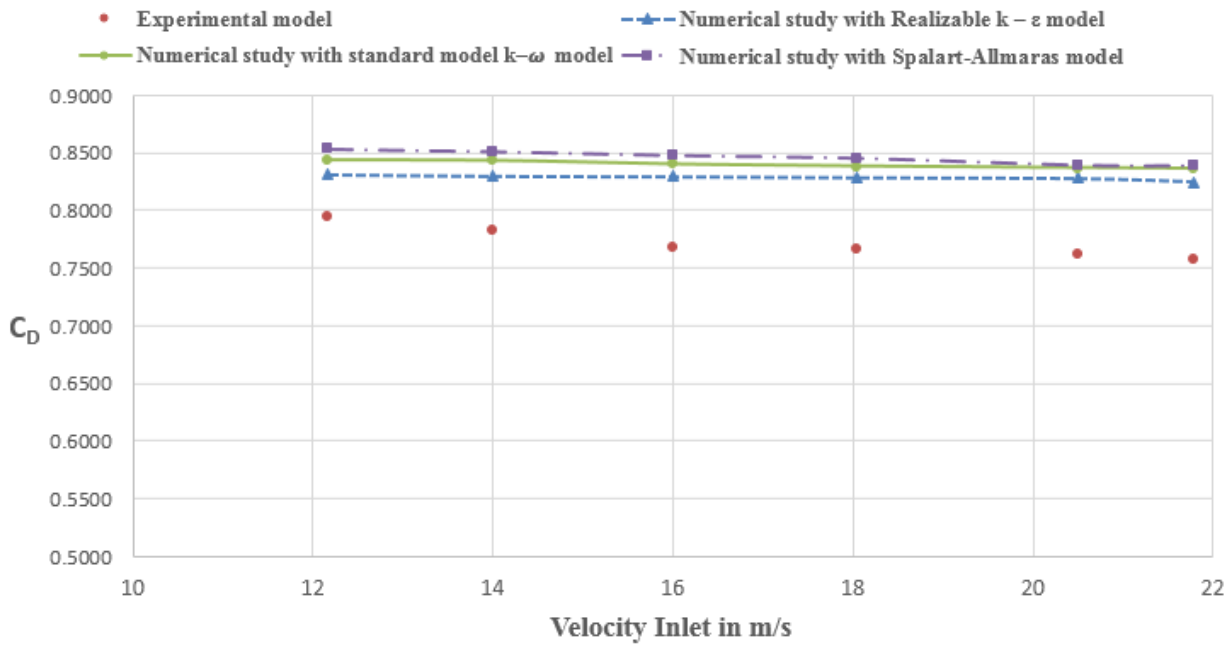

Fig. 7. Numerical results in comparison of C_D to corresponding experimental measurements.

3. MODELING, RESULTS AND DISCUSSION

The aerodynamic profiles and devices considered here are defined as for cabin and gab between cabin, and container. At first, a standard 3D Truck is modeled with aerodynamic profiles and devices with variable dimensions by Design modular, then the meshing is performed and boundary conditions are defined. The vehicle is assumed to have speed of 20 m/s (Re= 575321) at 300 K. The density of the air at the given temperature is ρ=1.225kg/m3, the static pressure is 101325 Pa and the viscosity is μ=1.7894×10-5 kg/m s.

3.1. Effect of Front Fillet Radius Ratio of cabin (FFRR)

First, it is investigated front fillet radius ratio of cabin (FFRR). The FFRR is defined the ratio of fillet radius (R1) and the height of front cabin (L1), as shown in figure 8. The FFRR is created with different ratio [0, 0.2, 0.4, 0.58 and 0.8] and it is illustrated the effect of it on the drag reduction.

Fig. 8. A standard heavy truck model with FFRR definitions as FFRR = [R_1/L_1].

The following figure 9 shows velocity vectors (m/s) on the standard 3D truck without and with FFRR at velocity 20 m/s. it is increases FFRR from 0 to 0.8, as shown in Figure 9(A) to Figure 9(D). At figure 9(A), the standard heavy truck without FFRR the vortices in front, around cabin and above container are significant that is indicated high drag force. At figure 9(B, C, D), the standard 3D truck with FFRR=0.2, 0.4 and 0.8 the vortices in front, around cabin and above container are decreased that is indicated a reduction in amount of drag force. The smallest vortices investigate on front, around cabin and above container with FFRR= 0.8 that is indicated a minimum amount of drag force.

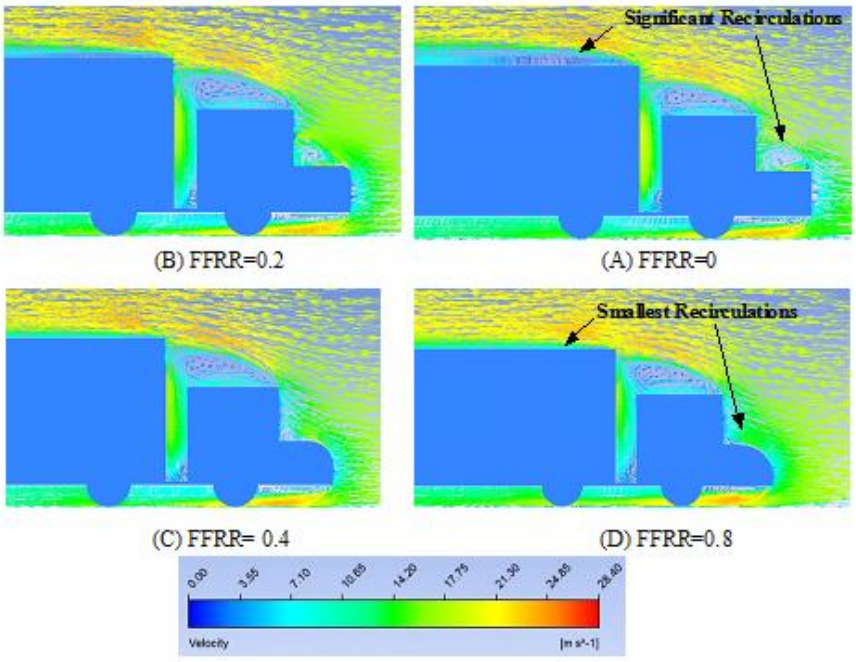

Fig. 9. Velocity vectors of A standard 3D truck model (A) FFRR=0, (B) FFRR=0.2,

(C) FFRR=0.4, (D) FFRR=0.8.

The standard 3D truck without aerodynamic profiles and devices at velocity 20 m/s has a drag coefficient about 0.82. Then, it is considered the effect of FFRR on drag force. The Results show C_D decreasing with increasing FFRR, as shown in figure 10. The improvement in C_D is about 17% at FFRR= 0.8.

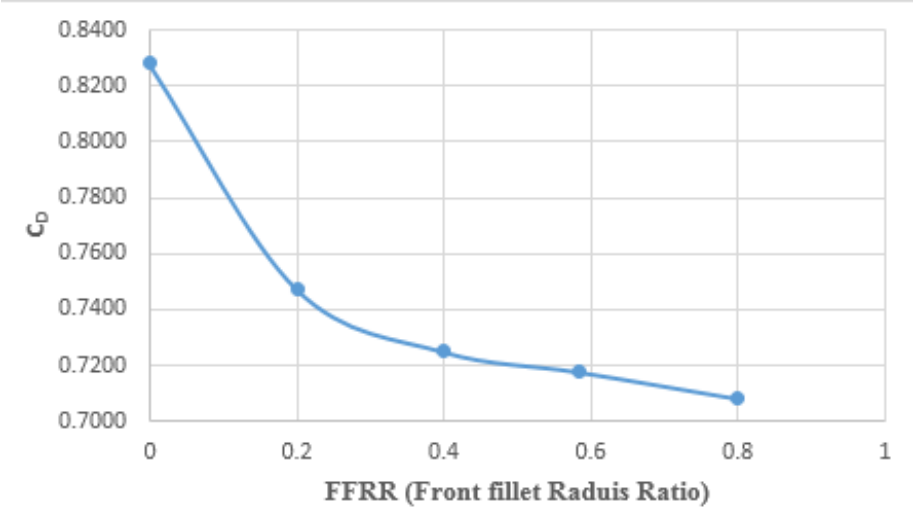

Fig. 10. Drag coefficient of a **standard** 3D Truck with FFRR [0, 0.2, 0.4, 0.58 and 0.8].

3.2. Effect of Mid Fillet Radius Ratio (MFRR)

Then a standard 3D truck with FFRR=0.8, it is investigated mid fillet radius ratio (MFRR). MFRR define the ratio of mid fillet radius (R2) and the height of front cabin (L1), as shown in figure 11. The MFRR is created with different ratio of [0, 0.2 and 0.4].

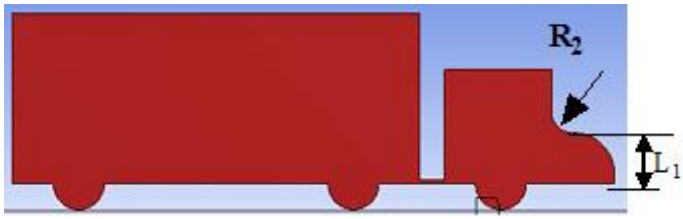

Fig. 11. A standard heavy truck model with MFRR = [R2/L1], [0, 0.2 and 0.4] and FFRR=0.8.

The following figure 12 shows a Velocity contours (m/s) and velocity vectors on the standard 3D truck with FFRR=0.8 and varies MFRR (0, 0.2 and 0.4) at velocity 20 m/s. The high intensity blue area (stagnation points and vortices regions in truck volume) located on the front and above surface of cabin due to sharp edge in front of cabin of the truck due to flow separation that is increasing a drag force. The following figure 12(A) show a static Velocity contours (m/s) and velocity vectors on the standard 3D truck with FFRR=0.8 and MFRR=0. The high intensity blue area is located in mid fillet. Figure 12(B) show a velocity contours (m/s) and velocity vectors on the standard 3D truck with FFRR=0.8 and MFRR=0.2. The high intensity blue area is decreased on mid fillet that is decreased the drag force. Figure 12(C) show a static Velocity contours (m/s) and velocity vectors on the standard 3D truck with FFRR=0.8 and MFRR=0.4. The high intensity blue area is increase on mid fillet that is increased the drag force. The effect of MFRR is very small in Drag reduction.

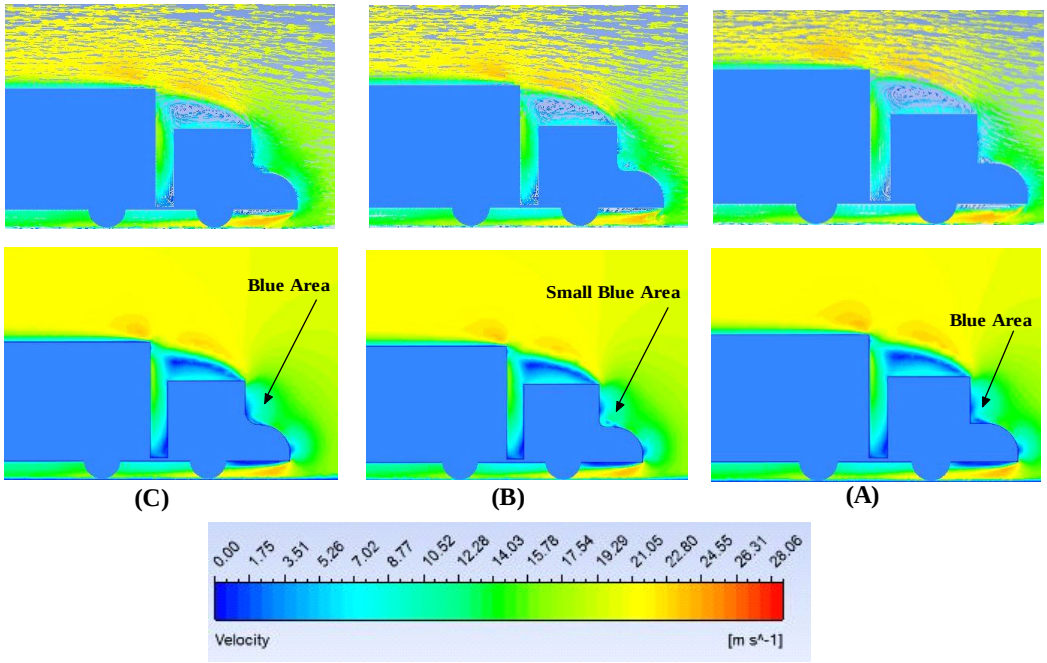

Fig. 12. Velocity contours and vectors of A standard 3D truck model with FFRR=0.8

(A) MFRR=0 (B) MFRR=0.2 (C) MFRR=0.4.

Then, It is illustrated the effect of MFRR with previous FFRR=0.8. The C_D is decreasing to optimum value and then increase with increasing MFRR up to optimum value. The improvement in C_D is about 0.75% by optimum MFRR=0.2 from previous cases, as shown in figure 13.

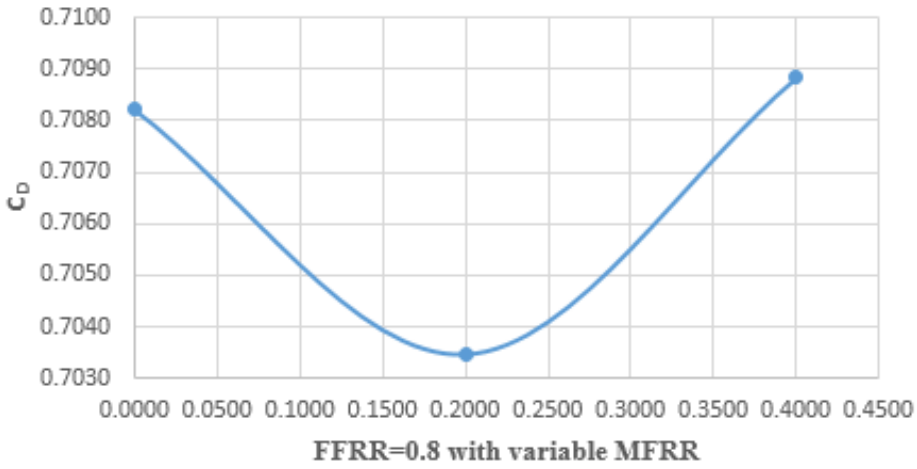

Fig. 13. Drag coefficient of a **standard** 3D Truck with FFRR=0.8 and MFRR [0, 0.2, 0.4, 0.58 and 0.8]

3.3. Effect of Top Fillet Radius Ratio (MFRR)

Then a standard 3D truck with FFRR=0.8 and MFRR=0.2 and Top Fillet Radius Ratio of cabin (TFRR) is investigated. The TFRR is defined the ratio of top fillet radius (R3) and the height of top front cabin (L2), as shown in figure 14. The TFRR is created with different ratio as [0, 0.2, 0.3, 0.6 and 0.8].

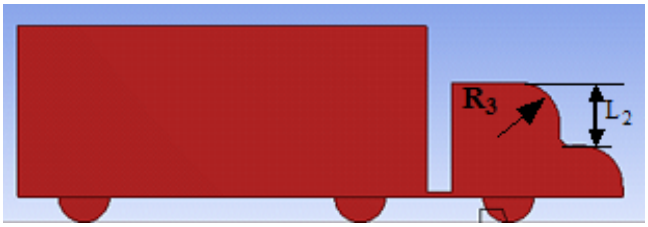

Fig. 14. A standard heavy truck model with TFRR = [R3/L2], [0, 0.2, 0.3, 0.6 and 0.8] MFRR=0.2 and FFRR=0.8.

The following figure 15 shows a Velocity contours (m/s) on the standard 3D truck with FFRR=0.8, MFRR=0.2 and varies TFRR [0, 0.2, 0.3, 0.6 and 0.8] at velocity 20 m/s, as shown in figure 15. From figure 15(A), It is illustrated the flow attached on top fillet with highest velocity and the flow lift off over above the container of truck due to Coandă effect. It is observed the high intensity blue area increasing on front and above container that is increasing the drag force. From figure 15 (B, C and D), It is increased TFRR that it observed the high intensity blue area decreasing on front and above container that is decreasing the drag force compare to case (A). The vortex is illustrated front and above truck container by using TFRR that is caused increasing in drag force.

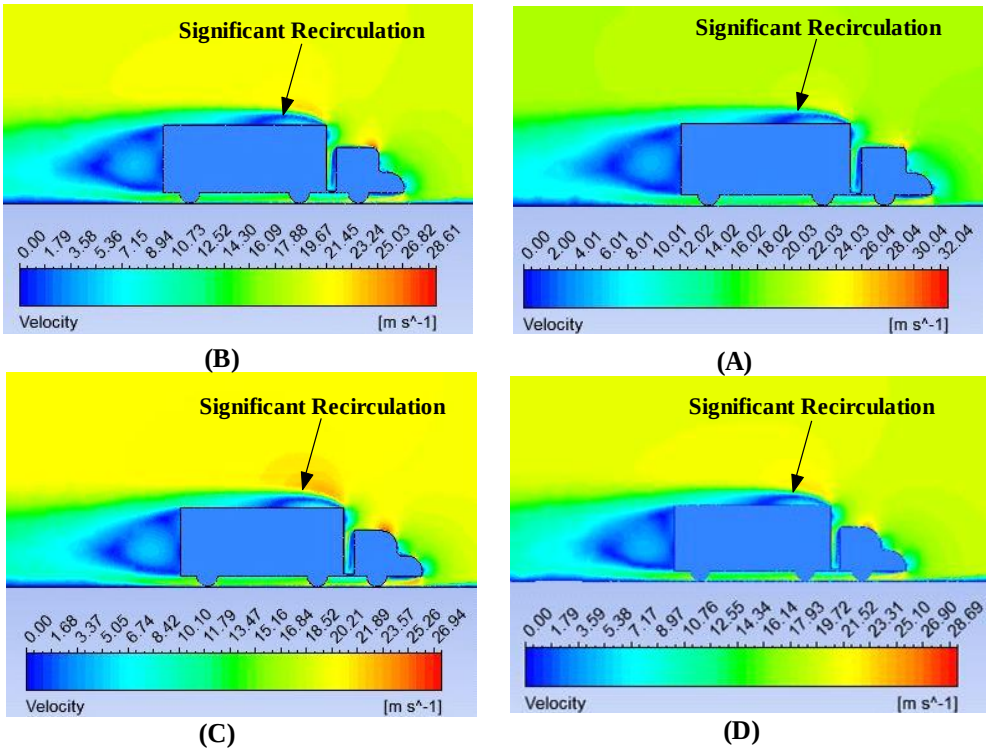

Fig. 15. Velocity contours of A standard 3D truck model with FFRR=0.8 and MFRR=0.2
(A) TFRR=0.2, (B) TFRR=0.3, (C) TFRR=0.6, (D) TFRR=0.8.

Then, It is illustrated the effect of TFRR with previous FFRR=0.8 and MFRR=0.2. The C_D is increasing from previous case with increasing TFRR due to Coandă effect that's increasing recirculation above the container. The TFRR has opposite effect on drag coefficient, as shown in figure 16.

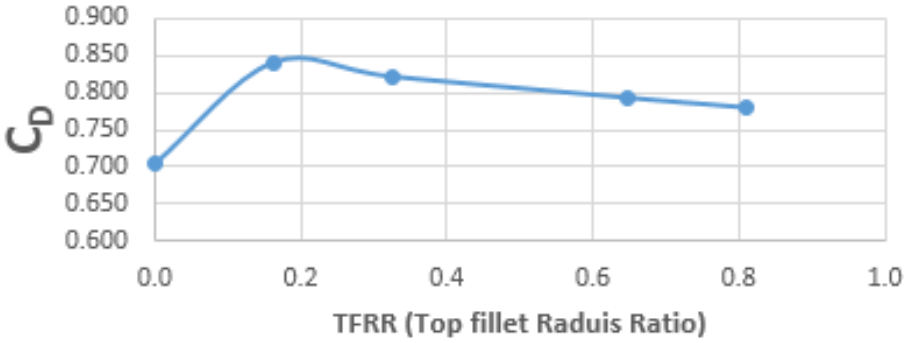

Fig. 16. Drag coefficient of a **standard** 3D Truck with FFRR=0.8 and MFRR [0, 0.2, 0.4, 0.58 and 0.8]

3.4. Effect of Cab Truck Angle Ratio (CTAR)

Then a standard 3D truck with FFRR=0.8, MFRR=0.2, Variation of TFRR and Cab Truck Angle Ratio (CTAR), is investigated. The CTAR is defined the ratio of cap truck angle (A_1) º over to 180 º, as shown in figure 17. At certain TFRR, It is investigated the effect of CTAR on the drag reduction. It is taken TFRR as 0.2, .03 and 0.6 and The CTAR is created with different Ratios [0.805, 0.833, 0.861, 0.889 and 0.916], as shown in figure 17.

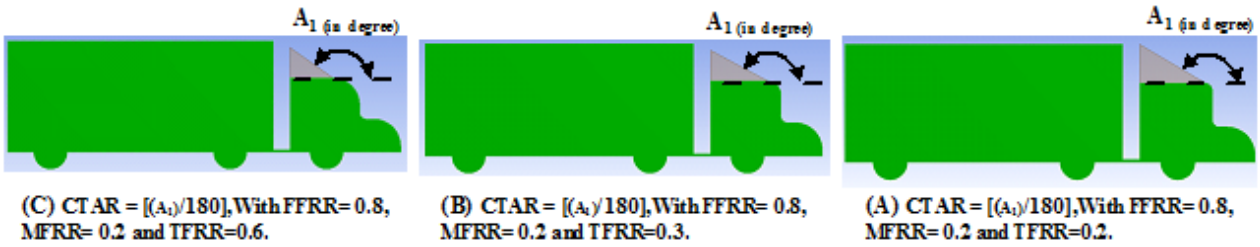

Fig. 17. A standard heavy truck model with TFRR = [R3/L2], [0, 0.2, 0.3, 0.6 and 0.8] MFRR=0.2 and FFRR=0.8.

The following figure 18 shows a Velocity vectors (m/s) and pressure contours (Pa) on the standard 3D truck with FFRR=0.8, MFRR=0.2, TFRR=0.2 and varies CTAR [0.805, 0.833, 0.861, 0.889 and 0.916] at velocity 20 m/s. from figure 18(A), It is taken CTAR as 0.805 (Cap truck angle as 145). The angle is low and the flow lift off over truck container surface and it illustrates significant vortices. It is caused reverse pressure and flow separation that's increase the drag force. The pressure is increasing in front of cabin truck and cab that is increasing the drag force. The high intensity red area (stagnation points in truck volume) value is 245.76 Pa. When it is increasing CTAR, the flow separation is decreasing. Figure 18(B) shows the optimum CTAR as 0.861 Cap truck angle as 155). It illustrates small vortices above container that is decreasing the drag force. The high intensity red area (stagnation points in truck volume) is decreased as 243.7 Pa in front and cap truck that is decreased the drag force. When it is increasing CTAR above the optimum value, the flow separation is increasing. Figure 18(C) shows CTAR as 0.916 Cap truck angle as 165). It illustrates high vortices above container that is increasing the drag force. The high intensity red area (stagnation points in truck volume) is increased in front of cabin and container that is increased the drag force.

According to Figure 19, the best angle of cab truck is obtained at certain TFRR and when the angle exceeds or lessens this angle, the drag coefficient increases because of disturbing the airflow. At TFRR as 0.2, the best CTAR is 0.861 and the drag coefficient is 0.6488. At TFRR as 0.3, the best CTAR is 0.805 and the drag coefficient is 0.6534. At TFRR as 0.6, the best CTAR is and the drag coefficient is 0.6672.the best case is the truck at TFRR=0.2 and CTAR=0.861that is made improvement in the drag about 9.92%.

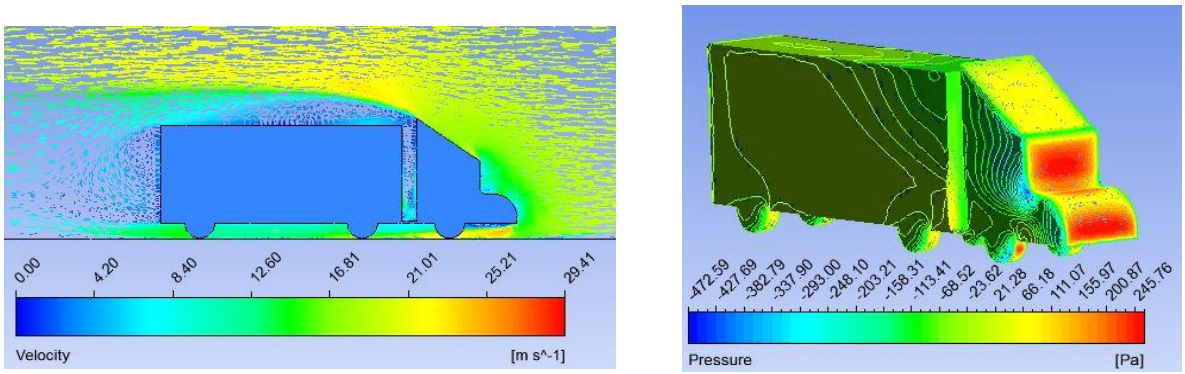

(A) CTAR= 0.805 and TFRR= 0.2

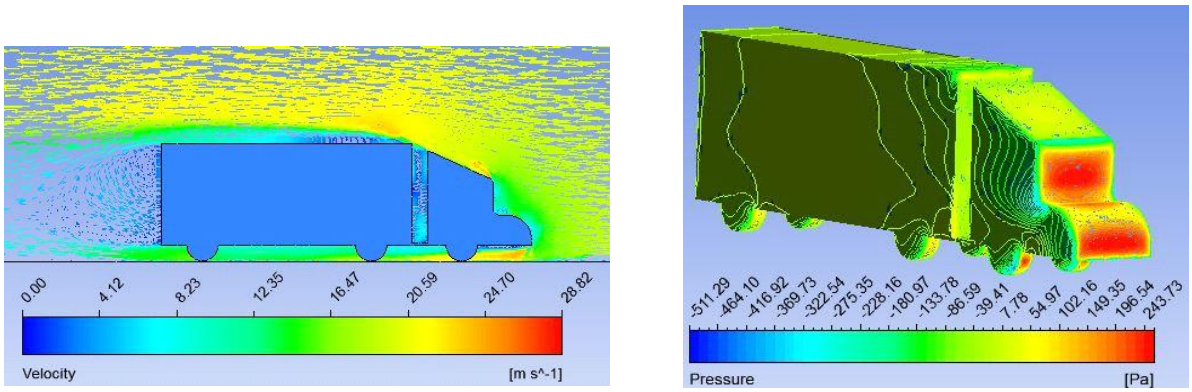

(B) CTAR= 0.861 and TFRR= 0.2

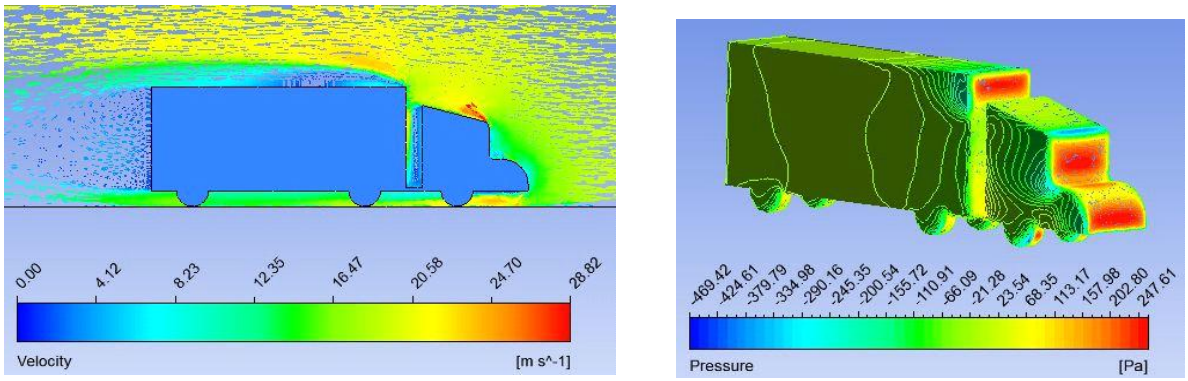

(C) CTAR= 0.916 and TFRR= 0.2

Fig. 18. Velocity vectors (m/s) and pressure contours (Pa) of A standard 3D truck model with FFRR=0.8, MFRR=0.2, TFRR=0.2.

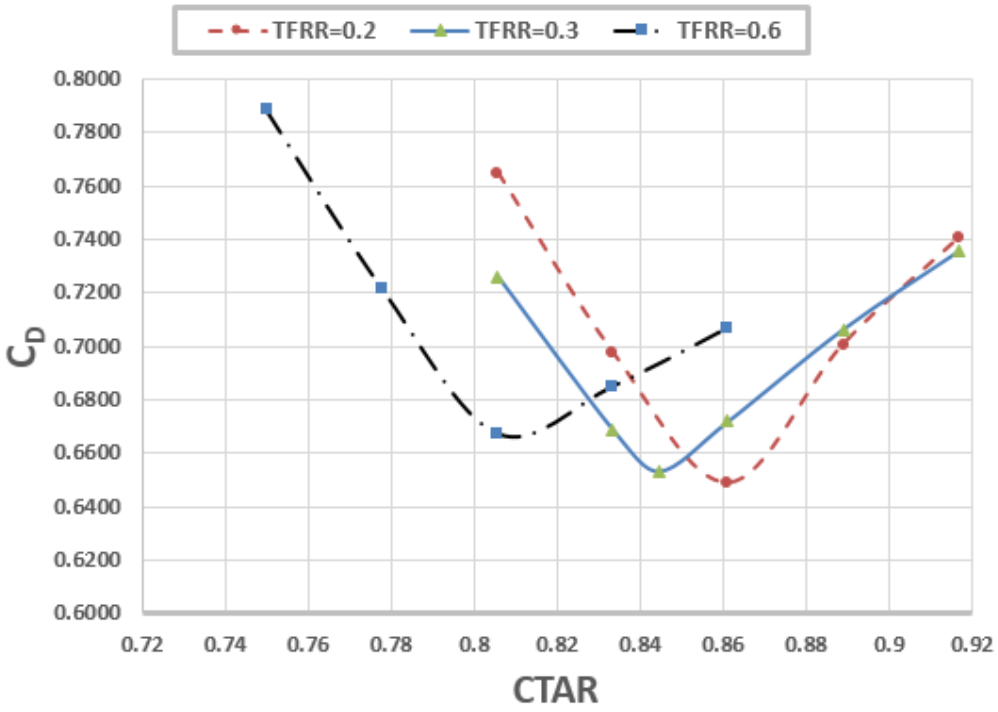

Fig. 19. Drag coefficient of a **standard** 3D Truck with FFRR=0.8, MFRR=0.2 and variable TFRR and CTAR.

3.5. Effect of Gap Length Device Ratio (GLDR)

Then a standard 3D truck with FFRR=0.8, MFRR=0.2, TFRR=0.2, CTAR=0.861 and variation of GLDR, is investigated. The GLDR is defined the ratio of gap length device over total gap length (L3), as shown in figure 20. The GLDR is created with different Ratios [0, 0.5 and 1].

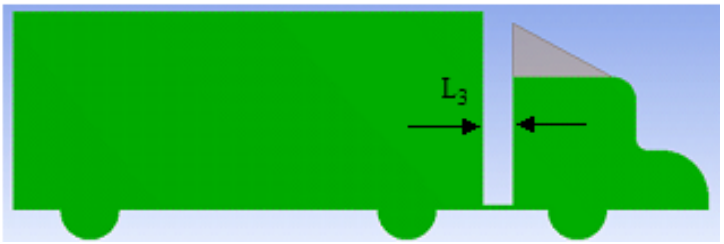

Fig. 20. A standard heavy truck model with FFRR=0.8, MFRR=0.2, TFRR =0.2, CTAR=0.861 and variation of GLDR.

The following figure 21 shows a Velocity vectors (m/s) on front and top view of the standard 3D truck with FFRR=0.8, MFRR=0.2, TFRR=0.2, CTAR 0.861 and GLDR of [0, 0.5 and 1] at velocity 20 m/s. from figure 21(A), It is taken GLDR as zero. It illustrates two significant vortices between cabin and container and above container that is increased the drag force. When it is increasing GLDR to 0.5, the vortices between cabin and container and above container are decreasing that is decreased the drag force, as shown in figure 21(B). From figure 21(C), the GLDR is one. The vortices between cabin and container and above container is dissipated that is decreasing the drag force.

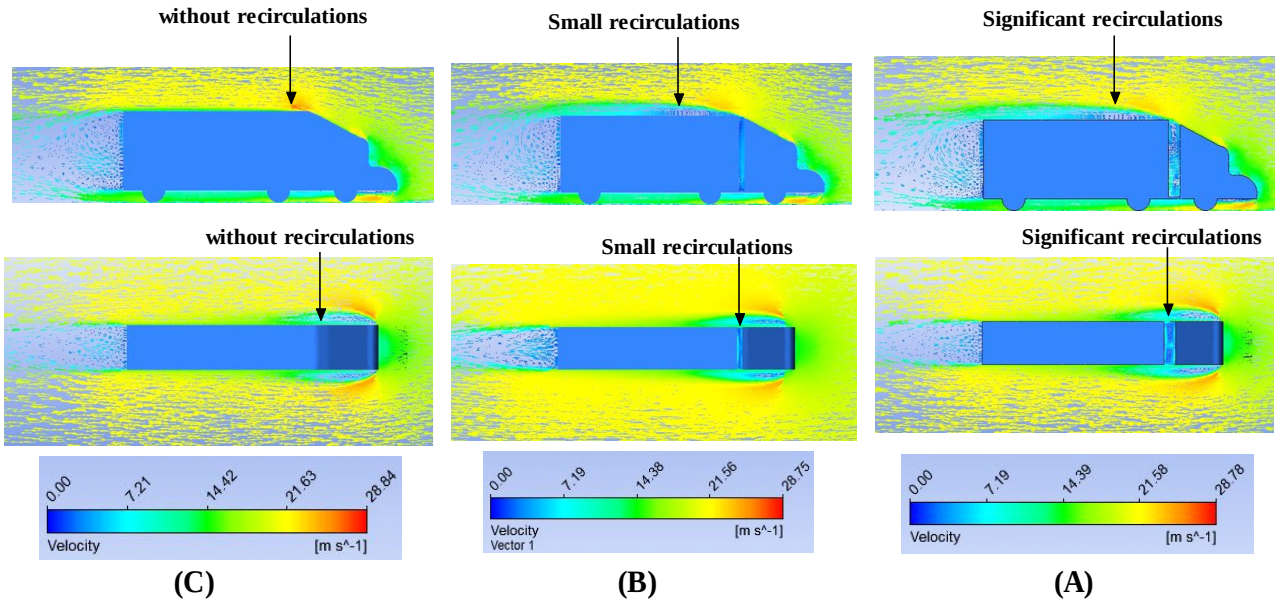

Fig. 21. Velocity vectors (m/s) of A standard 3D truck model with FFRR=0.8, MFRR=0.2, TFRR=0.2 and CTAR=0.861 (A) GLDR= 0, (B) GLDR= 0.5, (c) GLDR=1.

According to Figure 22, when it is increasing the GLDR from zero to one, the drag coefficient is increasing. At GLDR as one, the drag coefficient is improved by about 8.36% from previous case.

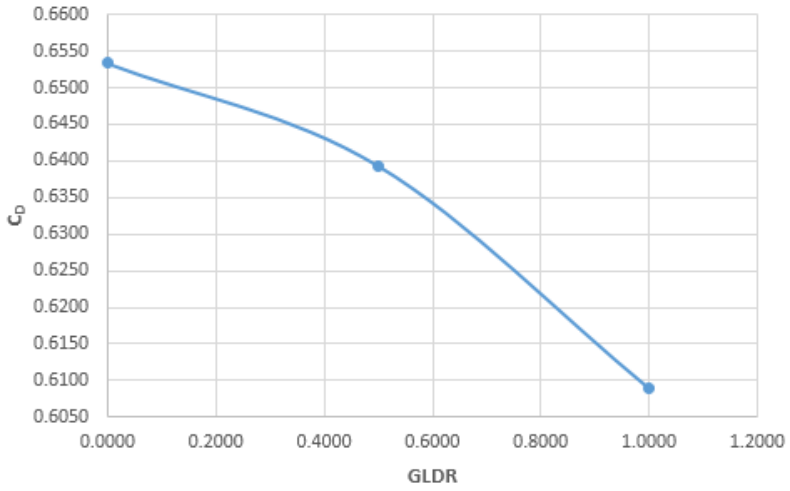

Fig. 22. Drag coefficient of a **standard** 3D Truck **at** FFRR=0.8**, MFRR=0.2, TFRR=0.2 and CTAR =0.861 with variation of GLDR.**

3.6. Effect of profiles and devices with best ratio on cabin of truck

Then a standard 3D truck with FFRR=0.8, MFRR=0.2, TFRR=0.2, CTAR=0.861 and GLDR=1, is investigated, as shown in fig. 23.

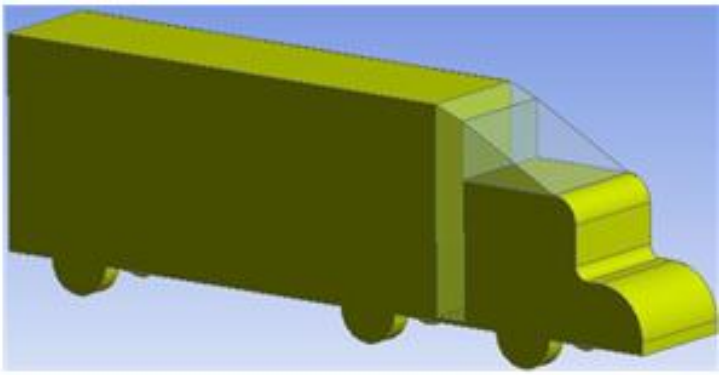

Fig. 23. A standard heavy truck model with FFRR=0.8, MFRR=0.2, TFRR =0.2, CTAR=0.861 and GLDR=1.

The following figure 24(A) shows Contours of turbulence kinetic energy (J/kg) around the standard 3D truck without aerodynamic profiles and devices at velocity 20 m/s. It is observed that, at the front, above cabin, gab between cabin and container, above container and at rear of container there is formation of high turbulence and formations of turbulent eddies because of adverse pressure gradient and the flow separation occur at edges. From figure 24(B), the flow around the truck body is smoothing and the turbulence and wake formation are decreases due to use all aerodynamic profiles and devices.

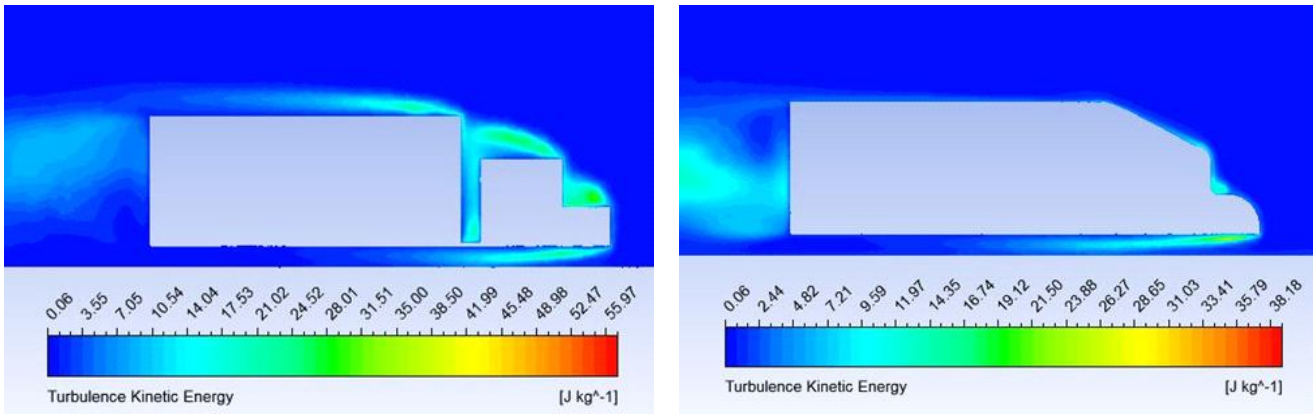

(A) (B)

Fig. 24. Turbulence Kinetic Energy (A) A standard 3D truck model without aerodynamic profiles and devices (B) A standard 3D truck model with all aerodynamic profiles and devices studied.

The following figure 25(A) shows the 3D stream lines around the standard 3D truck without aerodynamic profiles and devices at velocity 20 m/s. These stream lines show the big recirculation and the air flow is random and non-uniform around the truck volume. From figure 25(B), the recirculation is very small and the air flow is more uniform and aligned to the surface around the standard 3D truck with all aerodynamic profiles and devices, that's decreasing drag coefficient. With installing all aerodynamic profiles and devices at their best ratios and positions on cabin of a standard 3D truck, about 36.03 % drag reduction is enhanced compared to the standard 3D truck.

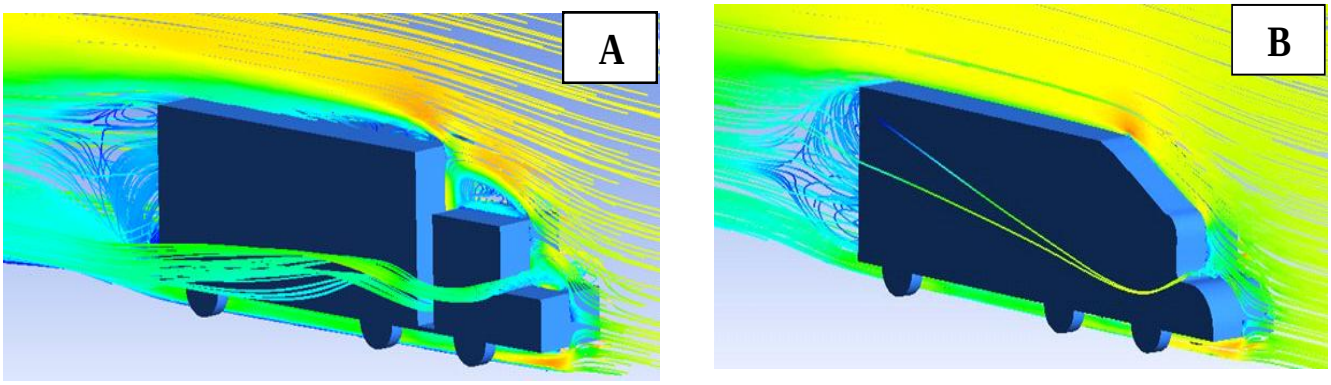

Fig. 25. 3D stream lines (A) A standard 3D truck model without aerodynamic profiles and devices, (B) A standard 3D truck model with all aerodynamic profiles and devices studied.

4. CONCLUSIONS

The aerodynamic profiles and devices attached on the cabin of truck have important impact on aerodynamic drag. The most effective aerodynamic profiles at the cabin is front fillet radius ratio (FFRR), by means of which, the drag coefficient decreases at FFRR= 0.8 by about 17%. The mid fillet radius ratio (MFRR) has low effect on drag reduction at optimum ratio by about 0.75%. The top fillet radius ratio (TFRR) has opposite effect on drag reduction due to Coandă Effect. The cap of truck ratio (CTAR) is utilized with TFRR has significant drag reduction at optimum angle. The optimum of CTAR is varied with different design of TFRR. At optimum CTAR with TFRR=0.2, FFRR=0.8 and MFRR=0.2, the drag reduction is about 27.67%. The increasing gap length device ratio (GLDR) that is decreasing in drag coefficient by about 8.36% at GLDR=1. With installing all aerodynamic profiles and devices at their optimized positions and dimensions on cabin of a standard heavy truck, about 36.03 % drag reduction is enhanced compared to the standard heavy truck.

REFERENCES

[1] PEVITT C, CHOWDURY H, MORIAAND H, ALAM F., "A computational simulation of aerodynamic drag reductions for heavy commercial vehicles". [C]// 18th Australasian Fluid Mechanics Conference Launceston. Australia, 2012: 191−194.

[2] HOWELL J P., "Aerodynamic drag reduction for low carbon vehicles". [M]// Sustainable Vehicle Technologies, Driving the Green Agenda. Woodhead, Elsevier publication, 2012: 145−154.

[3] MAHMOODI-K M, DAVOODABADI I, VIŠNJIĆ V, AFKAR A., "Stress and dynamic analysis of optimized trailer chassis" [J]. Technical Gazette, 2014, 21: 599−608.

[4] Wood, R.M., "Impact of advanced aerodynamic technology on transportation energy consumption". SAE Technical Paper 2004-01- 1306.

[5] KHALED M, ELHAGE H, HARAMBAT F, PEERHOSSAINI H., "Some innovative concepts for car drag reduction: A parametric analysis of aerodynamic forces on a simplified body" [J]. Journal of Wind Engineering and Industrial Aerodynamics, 2012, 107/108: 36−47.

[6] Davis SC, Williams SE, Boundy RG., "Transportation energy data book: edition 35." Oak Ridge: Center for Transportation Analysis Energy and Transportation Science Division, (2016).

[7] CHENG S Y, TSUBOKURA M, OKADA Y, NOUZAWA T, NAKASHIMA T, DOH D H., "Aerodynamic stability of road vehicles in dynamic pitching motion" [J]. Journal of Wind Engineering and Industrial Aerodynamics, 2013, 122: 146−156.

[8] KASSIM Z M, FILIPPONE A., "Fuel savings on a heavy vehicle via aerodynamic drag reduction". [J]. Transportation Research Part D: Transport and Environment, 2010, 15: 275−284.

[9] Khosravi M, khosravi F, Oveisi M, KhodayariBavil A.," Aerodynamic drag reduction of heavy vehicles using append devices by CFD analysis" J. Cent. South Univ. (2015) 22: 4645−4652.

[10] Chilbule C., Upadhyay A. and Mukkamala Y.," Analyzing the profile modification of truck-trailer to prune the aerodynamic drag and its repercussion on fuel consumption", 12th Global Congress on Manufacturing and Management, Procedia Engineering 97 (2014), 1208 – 1219.

[11] SELENBAS B, GUNES H, GOCMEN K.," An aerodynamic design and optimization of a heavy truck for drag reduction"., [C]// Proceedings of the ASME 2010 10th Biennial Conference on Engineering Systems Design and Analysis ESDA2010. Istanbul, Turkey, 2010: 121−129.

[12] ENGLAR R J. "Advanced aerodynamic devices to improve the performance, economics, handling and safety of heavy vehicles [R]." SAE Technical Paper, No. (2001)−01−2072.

[13] Versteeg, H., Malalasekera, W., "An Introduction to Computational Fluid Dynamics", The Finite Volume Method. Longman Scientific & Technical (1995).

[14] E. S. Abdelghany, Khalil, E. E., O. E. Abdelatif, and G. M. ElHarriry, (2016) COMPUTATIONAL ANALYSES OF AERODYNAMIC CHARACTERISTICS OF NACA653218airfoil. Proceedings, AIAA paper AIAA_2016_1_2307246.

[15] E. S. Abdelghany, Khalil, E. E., O. E. Abdelatif, and G. M. ElHarriry, (2016) THE CFD VALIDATION CODE FOR RECTANGULAR WING WITH NACA653218airfoil CROSS SECTION. Proceedings, AIAA paper AIAA_2016_1_2307247.

[16] E Abdelghany, A Alsayed, M Fouad, E Khalil, (2012) Effect of Shaped-Hole on Film Cooling Effectiveness of Gas Turbine Blade. Proceedings, 10th International Energy Conversion Engineering Conference, IECEC-2012- 3986.

[17] E Abdelghany, A Alsayed, M Fouad, E Khalil, (2012) On the Calculations of Flat Plate film cooling Effectiveness. Proceedings, IECEC paper IECEC-2012- 4231.

NOMENCLATURE

Symbol and Abbreviations	**Meaning and units**
A	Project area of truck (m2)
CFD	computational fluid dynamic
CD	Drag coefficient
CTAR	cab truck angle ratio
D	Drag force (N)
EWT	education wind tunnel
FAR	flap area ratio
FFAR	flat flap angle ratio
FFRR	front fillet radius ratio of cabin
FLR	flap length Ratio
GLDR	Gap length device Ratio
MFRR	mid fillet radius ratio
UFRR	under fillet radius Ratio
TFRR	top fillet radius ratio of cabin